Proceedings of the 2003 IEEE
International Conference on Robotics & Automation
Taipei, Taiwan, September 14-19, 2003

Actively Servoed Multi-Axis Microforce Sensors

Yu Sun*, D.P. Potasek*, D. Piyabongkarn*, R. Rajamani*, and B.J. Nelson†

*Department of Mechanical Engineering, University of Minnesota, Minneapolis, U.S.A.
E-mail: yus@me.umn.edu

†Institute of Robotics and Intelligent Systems, ETH Zurich, Switzerland
E-mail: bradley.nelson@iris.mavt.ethz.ch

***Abstract*— This paper presents design, fabrication, and calibration results of MEMS-based two-axis capacitive force sensors capable of resolving forces up to 490μN with a resolution of 0.01μN in x, and up to 900μN with a resolution of 0.24μN in y in the passive mode. Electrostatic microactuators are integrated to enable the force sensors to operate in an actively servoed mode, in which system stiffness is modulated using force compensation, greatly increasing force measurement dynamic ranges. When the microforce sensor is actively servoed, an externally applied force is balanced by the electrostatic forces generated by the electrostatic microactuators within the sensor. The movable parts of the sensor are maintained in the equilibrium position, making the system a regulator system. The force measurement is obtained by interpreting the actuation voltages. Probes of different shapes are integrated with the sensors for micromanipulation. Other types of end-effectors, such as microgrippers and microneedles for different micromanipulation tasks can be integrated by modifying the fabrication sequence. The current application of the force sensors is for providing real-time force feedback during microrobotic cell manipulation.**

I. Introduction

When autonomously manipulating objects, force feedback almost always improves the speed and robustness with which the manipulation task is performed. When manipulating objects ranging in size from microns to nanometers, force information is difficult to measure and is typically obtained along a single axis using laser-based optical force measurement techniques or piezoresistive devices. Recent advances in microbiology such as cloning require increasingly complex micromanipulation strategies for manipulating individual biological cells. Although multi-axis force sensing capabilities would be useful for handling cells by providing information on probing forces as well as tangential forces generated by improperly aligned cell probes, no sensors capable of multi-axis force sensing at the force scales required are available. This paper describes the design of a two-axis capacitive cellular force sensor for microrobotic cell manipulation that is actively servoed, making the impedance variable and increasing the force measurement dynamic range.

For cellular force measurement, cantilevers are the most frequently implemented MEMS devices. The main sensing mechanisms used with cantilevers are optical, piezoresistive, and piezoelectric methods. Cantilever-based optical force sensors and piezoresistive force sensors have been reported for cellular force measurement [1][2][3][4][5]. Cantilever-based optical force measurement often uses atomic force microscopy (AFM) techniques. There are four limitations restricting AFM use in cellular force measurement during manipulation. First, different types of end-effectors such as microneedles are difficult, if possible, to be integrated in the AFM system. Second, a major requirement in AFM measurement is that a complex transmit-receive setup is required. This setup places a high demand on optical alignment and adjustment. The surface of the cantilever must also be sufficiently reflective to achieve high accuracy. Third, an important system limitation is that the photodiode can only detect a small range of deflection. This constrains the force measurement range. Forth, when an AFM is used in aqueous mediums where biological cells survive, the reflection and refraction of the transmitted light make the accuracy of cellular force measurements problematic.

Even though widely used, almost all existing cantilever-based cellular force sensors are only capable of measuring forces perpendicular to the sensor plane. To provide multi-axis force information and avoid the limitations of atomic force microscopy, a multi-axis capacitive cellular force sensor has been designed and fabricated. To convert force into a relatively large capacitance change, the capacitive cellular force sensor employs an interdigitated transverse comb drive structure. A high-yield process using Deep Reactive Ion Etching (DRIE) on Silicon-On-Insulator (SOI) was developed to form high aspect ratio suspending interdigitated comb drive structures. The high aspect ratio structures together with the transverse movement mode of the comb drives greatly increase device sensitivity.

End-effectors of two shapes, a cylindrical die and a sharp tip have been integrated on the force sensors for cell manipulation. For applications such as cell grasping and injection, microgrippers and microneedles can be integrated on the force sensors by modifying the fabrication sequence.

The concept of force-balance or force-compensation has been widely adopted in both macro-scale and micro-scale sensors, mainly in seismometers [6][7], accelerometers [8][9][10][11][12][13] and pressure sensors [14][15]. In such devices, a feedback loop is formed when an electromagnetic force [6][7] or electrostatic force [8][9][10][11][12][13][14][15] is generated by an actuator

within the sensor to balance the externally applied load, making the movable part of the sensor remain in its equilibrium position. Because of the integration of the servo mechanism, the sensors using the force-balance concept are classified as servo sensors or active sensors compared to conventional passive sensors.

Among many other advantages of active sensors, dynamic range can be extended. Further, the direct influence of material properties on the sensor output can be removed when the control loop gain is sufficiently high. However, the output is dependent on the actuator characteristics. Therefore, an actuator with a transfer function independent of material properties is desirable, as is the case in parallel-plate and transverse comb drive electrostatic actuators [16].

Though macro-scale active force sensors have been developed [17], MEMS-based active force sensors sensing sub-micro-Newton forces have not been reported. The microforce sensors presented in this paper can be servoed to operate in the active mode. When the sensor is actively servoed, an externally applied force is balanced by the electrostatic forces generated by the electrostatic microactuators within the sensor, which essentially modulates device stiffness. Force measurement is obtained by interpreting the actuation voltages. Experimental results demonstrate that the force sensor operating in the active mode has a much larger dynamic range than in the passive mode. Thus, one device of low stiffness is capable of measuring a large range of forces without the need of switching to higher stiffness devices.

In Section II, the design, fabrication, and calibration results in the passive mode of the microforce sensors are described. The microactuation analysis, control scheme, and active force sensing experimental results are presented in Section III. Conclusions are given in Section IV.

II. Sensor Design, Fabrication, and Calibration

A. Microforce Sensor Design and Analysis

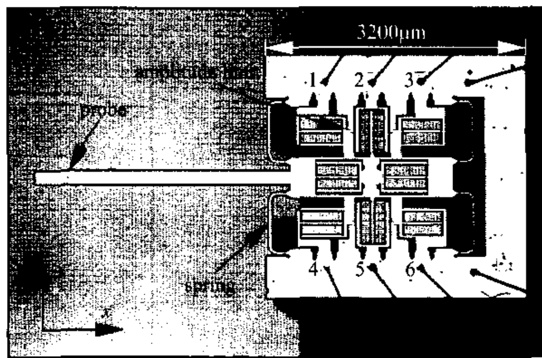

Fig. 1. A wire-bonded multi-axis force sensor.

Figure 1 shows a force sensor bonded to a readout circuit board. The constrained outer frame and the inner movable plate are connected by four curved springs. A load applied on the probe causes the movable plate to move, changing the gap between each pair of the interdigitated comb capacitors. Consequently, the total capacitance change resolves the applied force. To make the force sensor capable of resolving forces in both x and y directions, the interdigitated capacitors are configured to be orthogonal to each other. Comb drive 1, 3, 4, and 6 resolve forces in x, and comb drive 2 and 5 resolve forces in y.

The spring dimensions determine the system stiffness. Structural analysis was performed numerically. The force-deflection model of the spring in x and y is

$$\delta = \lambda \times \frac{F}{Et^3h} \tag{1}$$

where δ is the deflection; F is the force acting on the springs in the direction of δ; $E = 125GPa$ is the Youngs modulus of silicon; $t = 3, 5, 7, 10\mu m$ is the width of the springs; $h = 50\mu m$ is the height of the springs; $\lambda = 2.359 \times 10^{-10} m^3$ in x, and $\lambda = 7.102 \times 10^{-12} m^3$ in y. By varying the dimensions of the springs to change device stiffness, a large range of forces can be resolved.

Electrostatic analysis was conducted using finite element method. In the simulations, the fringing fields were taken into account. Figure 2 shows the combined structural and electrostatic analysis results.

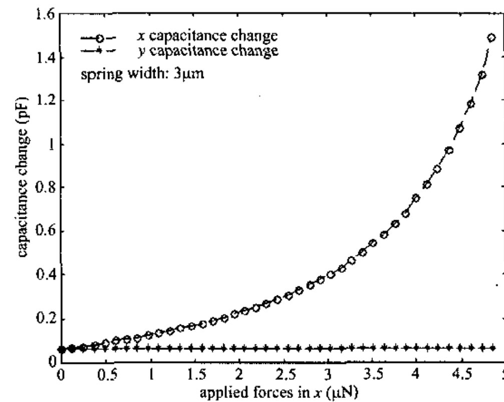

Fig. 2. Capacitance change when forces are applied in x.

B. Microforce Sensor Fabrication

The main microfabrication process is illustrated in Figure 3.

Step 1. Start from a double polished P-type wafer with crystal orientation of <100>.

Step 2. LPCVD (Low Pressure Chemical Vapor Deposition) $1\mu m$ SiO_2.

Step 3. Fusion bond the wafer with SiO_2 with another P-type wafer.

Step 4. CMP (Chemical Mechanical Polishing) the top wafer down to $50\mu m$; this forms an SOI (silicon-on-insulator) wafer.

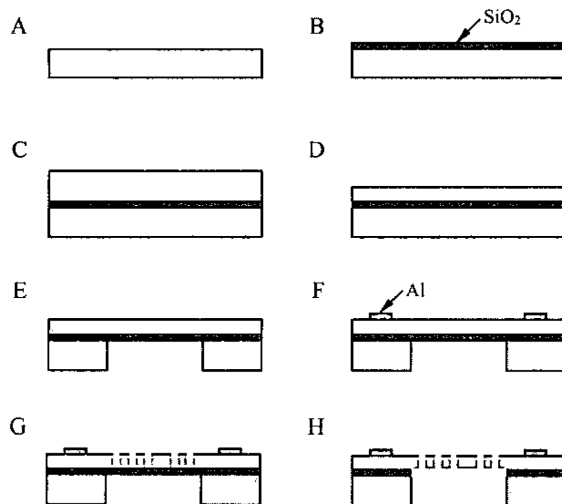

Fig. 3. Fabrication sequence.

Step 5. DRIE (Deep Reactive Ion Etching) to form the features on the back side such as the outer frame and movable plates. The buried $1\mu m$ SiO_2 layer acts as an etch stop layer and also as an insulator between the capacitors.
Step 6. E-beam evaporate Al to form Ohmic contacts; liftoff to pattern Al.
Step 7. DRIE the top side to form capacitive comb fingers and curved springs; The devices were connected to the device wafer only by the buried SiO_2 layer.
Step 8. RIE (Reactive Ion Etching) to remove the buried SiO_2 layer; The released devices placed themselves on a carrier dummy wafer below the device wafer, and then were picked up individually from the carrier dummy wafer. The dice-free release process protects fragile structures from being damaged.

Figure 4 shows a completed device. Wire bonding and packaging were subsequently undertaken.

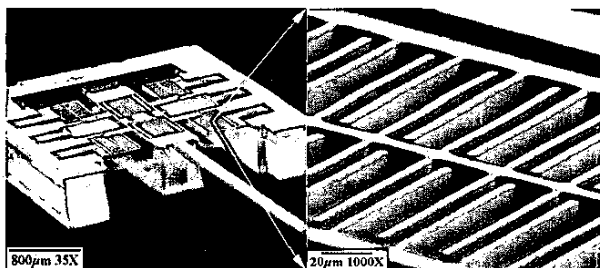

Fig. 4. SEM micrograph of a completed device and offset comb drive.

Besides the probes with rectangular tips, end-effectors with a sharp tip, as shown in Figure 5 are also integrated on the force sensors for micromanipulation. The design and fabrication sequence can be readily modified to integrate other types of end-effectors, such as microgrippers and microneedles for different micromanipulation tasks.

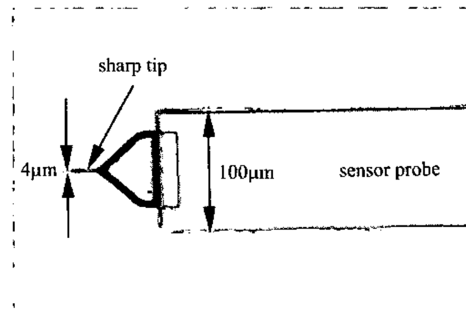

Fig. 5. Integrated sharp tip.

C. Sensor Calibration

A capacitive readout ASIC, the MS3110 from MicroSensors with a resolution of $4.0aF/\sqrt{Hz}$, was used to convert capacitance change into voltage change. The relationship between input capacitance change and the output voltage is strictly linear. The force sensor was wired bonded to a circuit board. A micro-controller programs the capacitance readout IC MS3110 so that the internal registers can be trimmed for accurate measurements. An on-board 16-bit A/D converter converts the analog output of the MS3110 into digital signals to decrease the voltage drop and noise. The converted digital signals are received through the micro-controller by a host PC.

Calibration was conducted using calibrated piezoresistive cantilevers. The stiffness of the cantilevers varies from $0.1\mu N/\mu m$ to $1714.29\mu N/\mu m$. The cantilevers were mounted on a 3-DOF microrobot in which the XYZ axes each has a travel of $2.54cm$ with a step resolution of $40nm$, applying a known force to the probe of the force sensor in a known direction, causing gap changes and capacitance changes for calibration.

Table I lists the structural calibration results of the devices with various spring widths.

TABLE I
STIFFNESS OF DEVICES WITH DIFFERENT SPRING WIDTH.

spring width (μm)	stiffness k_x (N/m)	stiffness k_y (N/m)
3	1.136	24.106
5	5.248	110.753
7	14.375	301.469
10	38.46	867.862

Calibration results for devices with $3\mu m$ wide springs are shown in Figure 6. Devices with four different spring widths have similar electrostatic properties (i.e., the relationship between gap change and capacitance change). They differ

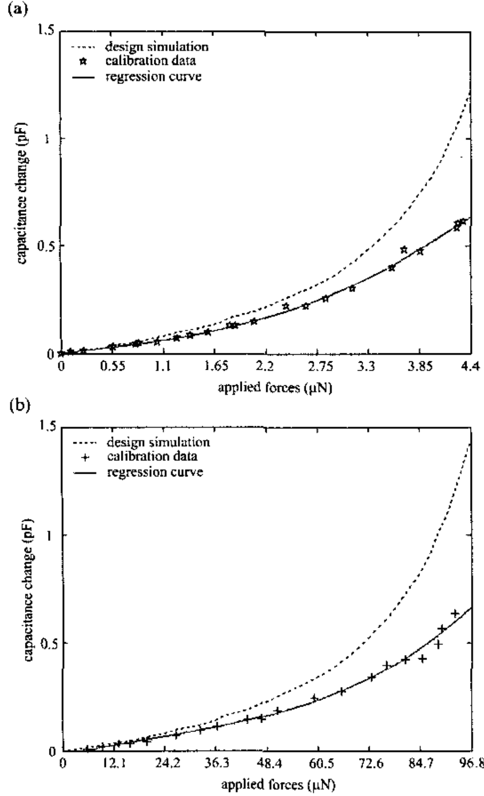

Fig. 6. Calibration results for devices with $3\mu m$ springs. (a) in x; (b) in y.

only in mechanical properties (i.e., the relationship between applied forces and resulting gap changes). The lower capacitance change is mainly due to the parasitic capacitance in series with the sensing comb capacitors, such as from poor Ohmic contact.

The microforce sensors with four different spring widths are capable of resolving forces up to $490\mu N$ with a resolution of $0.01\mu N$ in x (1σ), and up to $900\mu N$ with a resolution of $0.24\mu N$ (1σ) in y.

III. Actively Servoed Microforce Sensor

When manipulating objects of various mechanical impedance, force sensors of different stiffness need to be used. For example, sensors with $3\mu m$ wide springs can only measure forces up to $5\mu N$ when the mechanical amplitude limit stops further motion of the movable parts of the sensor. To measure forces larger than $5\mu N$, stiffer sensors have to be used. Continuously switching from one device to another is difficult and tedious, which is even impossible for manipulation tasks in an unknown environment. When the sensor is servoed to operate in the active mode, device stiffness is modulated to balance externally applied forces. This increases the force measurement dynamic range, making the same device capable of measuring a large range of forces without the need of switching devices.

When an external force is applied on the sensor tip, the resulting gap/position change is sensed by the comb drives serving as capacitive position sensors. Upon the gap change, a controller applies an appropriate voltage to the electrostatic microactuators within the sensor to generate forces to balance the applied force, bringing the movable parts of the sensor back to the equilibrium position from the slight gap offset. The force measurement is obtained by interpreting controller output voltages that include the applied force information. Theoretically, by applying infinitely large voltages to the electrostatic microactuators within the force sensor, the sensor can measure/balance infinitely large externally applied forces.

In the experiments, a force sensor with $3\mu m$ wide springs was servoed to resolve forces in x to illustrate the active force sensing mechanism. Comb drive 1 and 4 shown in Figure 1 were used for position sensing, and comb drive 3 and 6 were actuated to balance the externally applied forces.

A. Microactuation Analysis

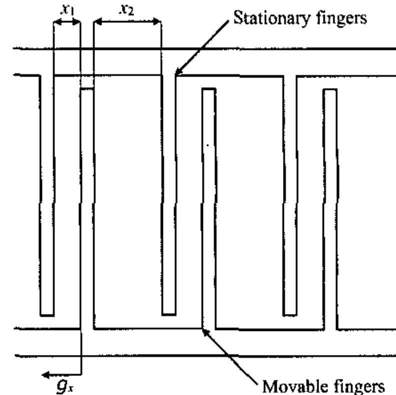

Fig. 7. Offset comb drive model in x.

The offset comb drives used in the design are modelled along the x direction as shown in Figure 7, where g_x is the displacement of the movable fingers from the equilibrium position. When the force sensor operates in the active mode, the movable parts of the sensors remain in the equilibrium position, i.e., g_x is kept at zero. The electrostatic force acting on the movable comb fingers in x is

$$F_e = \frac{1}{2}NK\epsilon A[\frac{(x_1+x_2)(x_2-x_1+2g_x)}{(x_1-g_x)^2(x_2+g_x)^2}]V_x^2 \quad (2)$$

where N is the number of parallel capacitor pairs; K is the dielectric constant for the material (for air $K = 1$); $\epsilon = 8.8542 \times 10^{-12}C^2/(N \times m^2)$ is the permittivity of free space; $x_1 = 5\mu m$; $x_2 = 12\mu m$; $A = 7500\mu m^2$ is the

overlapping area of each finger pair; and V_x is the applied actuation voltage in x. This generated electrostatic force balances externally applied forces. An identical formulation applies to the y direction.

B. Force Sensing Using Force Compensation

Figure 8 shows the real-time control system setup for active force sensing. The *xPC*-Target1.3 from MathWorks was used to generate the real-time operating system kernel. An I/O board (National Instrument PCI-MIO-16E-4) performs sampling at a frequency of $20KHz$.

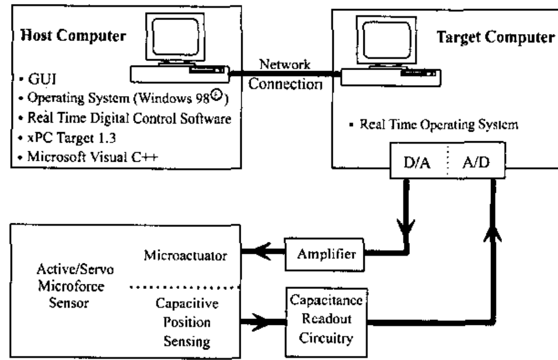

Fig. 8. Real-time control system setup.

The microactuators of the active force sensor are modelled individually in x and y as two independent spring-mass-damper systems, where in x

$$m\ddot{g}_x + 2\zeta_x\sqrt{k_x m}\dot{g}_x + k_x g_x \quad = F_e \tag{3}$$

The system consists of the linear equation of motion ($EOM = 1/m(s^2+2\zeta_x\omega_{nx}s+\omega_{nx}^2)$) and nonlinear electrostatic forces F_e given in (2). An identical formulation applies to the y direction.

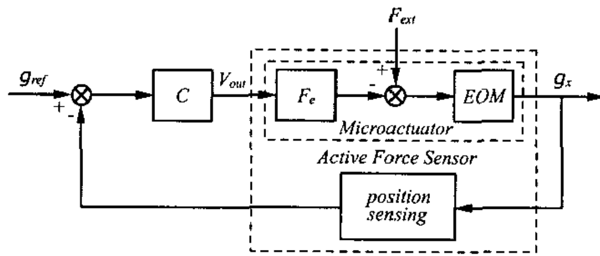

Fig. 9. Active force sensing control scheme.

A proportional-integral ($C(s) = K_p + K_i/s$) PI control architecture shown in Figure 9 was implemented. A nonlinear controller for nonlinearity compensation is not needed because system nonlinearity is trivial when the system operates about the equilibrium position. The control task is equivalent to rejecting the disturbance, i.e., the externally applied forces F_{ext} to track a zero position change from equilibrium. Thus this system holding the output steady ($g_x = g_{ref} = 0\mu m$) against unknown disturbances is a regulator system. When an external force is applied, a slight position offset is sensed by the capacitive position sensors. Consequently, the PI controller controls the electrostatic microactuators to generate electrostatic forces to balance the external force, maintaining the movable parts of the sensor in the equilibrium position. The balancing force, calculated through the controller output V_{out} and (2) is the measurement of the externally applied force F_{ext}.

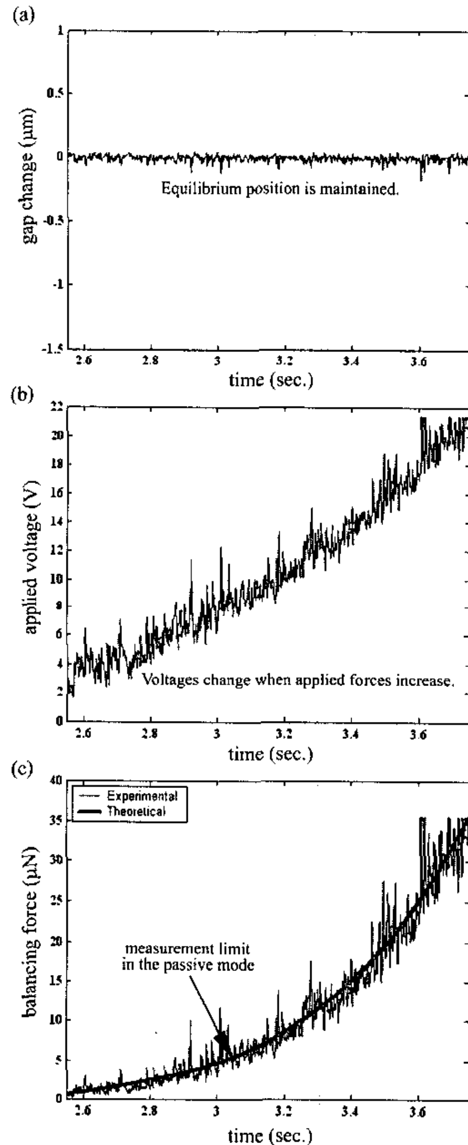

Fig. 10. Active force sensing experimental results with time varying external forces. (a) gap change; (b) applied voltages; (c) balancing forces - force measurement results.

Figure 10 shows the constant gap, applied voltage change, and force measurement results in active force sensing. Experimental results demonstrate that the equilibrium position is maintained when external forces are applied. With up to $20V$ servoing voltages, the dynamic range of the force sensor with $3\mu m$ wide springs is increased from $5\mu N$ in the passive mode to $35\mu N$ in the active mode. Higher measurement range can be achieved when larger servoing voltages are supplied.

In robotic manipulation, matching manipulator impedance with the impedance of the manipulated object is desired to maximize power transmission and to achieve compliant motion [18]. However, for cell membrane force sensing during microrobotic cell manipulation shown in Figure 11, the impedance of the force sensor mounted on a microrobot is desired to be large before puncturing the cell membrane, and small after membrane puncture to protect the force sensor from being broken by colliding into the high-impedance holding pipette. Thus, the adjustable impedance characteristic of the presented force sensor provides much flexibility in cell manipulation.

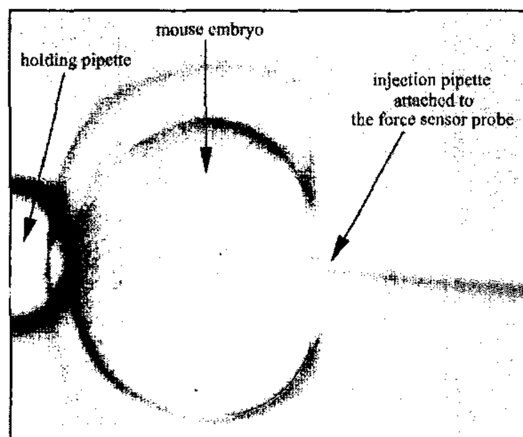

Fig. 11. Cell membrane force sensing during manipulation.

IV. Conclusions

MEMS-based two-axis capacitive force sensors, in the passive mode capable of resolving forces up to $490\mu N$ with a resolution of $0.01\mu N$ in x, and up to $900\mu N$ with a resolution of $0.24\mu N$ in y are presented. The design, fabrication, and calibration results are described. The force sensors' stiffness are modulated using force compensation, made possible by the built-in electrostatic microactuators. Experimental results have demonstrated greatly increased force measurement dynamic ranges when the force sensors operate as active/servo sensors. The on-going research using the force sensors is to characterize mouse egg cell and embryo membrane mechanical properties to provide insight into cell injection studies and facilitate complex microrobotic cell manipulation tasks.

V. Acknowledgement

This work was supported in part by the National Science Foundation through Grant Number 0208564. The authors would like to thank A. Sezen for the valuable discussions on the project.

References

[1] M.E. Fauver, D.L. Dunaway, D.H. Lillenfeld, H.G. Craighead, and G.H. Pollack, "Microfabricated cantilevers for measurement of subcellular and molecular forces," *IEEE Transactions on Biomedical Engineering*, vol. 45, pp. 891–898, 1998.

[2] G. Lin, K.S. Pister, and K.P. Roos, "Novel microelectromechanical system force transducer to quantify contractile characteristics from isolated cardiac muscle cells," *Journal of the Electrochemical Society*, vol. 142, pp. 31–33, 1995.

[3] G. Lin, K.S. Pister, and K.P. Roos, "Surface micromachined polysilicon heart cell force transducer," *Journal of Microelectromechanical Systems*, vol. 9, pp. 9–17, 2000.

[4] G.T. Charras, P.P. Lehenkari, and M.A. Horton, "Atomic force microscopy can be used to mechanically stimulate osteoblasts and evaluate cellular strain distribution," *Ultramicroscopy*, vol. 86, pp. 85–95, 2001.

[5] G.G. Guilbault and J.H. Luong, "Biosensors: current status and future possibilities," *Ion Selective Electrode Review*, vol. 11, pp. 3–11, 1989.

[6] M.J. Usher, C. Guralp, and R.F. Burch, "The design of miniature wideband seismometers," *Geophys. J.*, vol. 55, pp. 605–613, 1978.

[7] E. Wielandt, and G. Streckeisen, "The leaf-spring seismometer: design and performance," *Bull. Seism. Soc. Am.*, vol. 72, pp. 2349–2367, 1982.

[8] W.J. Yun, R.T. Howe, and P.R. Gray, "Surface micromachined, digitally force-balanced accelerometer with integrated CMOS detection circuitry," *IEEE Solid-State Sensor and Actuator Workshop, 5th Technical Digest.*, pp. 126–131, 1992.

[9] L. Zimmermann, J.Ph. Ebersohl, F.Le Hung, J.P. Berry, F. Baillieu, P. Rey, B. Diem, S. Renard, and P. Caillat, "Airbag application: A microsystem including a silicon capacitive accelerometer, CMOS switched capacitor electronics and true self-test capability," *Sensors and Actuators A: Physical*, vol. 46, pp. 190–195, 1995.

[10] K.H.-L. Chau, S.R. Lewis, Y. Zhao, S.F. Bart, R.G. Marcheselli, and R.T. Howe, "An integrated force-balanced capacitive accelerometer for low-g applications," *Sensors and Actuators A: Physical*, vol. 54, pp. 472–476, 1996.

[11] B.P. van Drieenhuizen, N.I. Maluf, I.E. Opris, and G.T.A. Kovacs, "Force-balanced accelerometer with mG resolution fabricated using Silicon Fusion Bonding and Deep Reactive Ion Etching," *1997 Solid State Sensors and Actuators, TRANSDUCERS '97*, Chicago, pp. 1229–1230, 1997.

[12] M.A. Lemkin, B.E. Boser, D. Auslander, and J.H. Smith, "A 3-axis force balanced accelerometer using a single proof-mass," *1997 Solid State Sensors and Actuators, TRANSDUCERS '97*, Chicago, pp. 1185–1188, 1997.

[13] I.Y. Park, C.W. Lee, H.S. Jang, Y.S. Oh, and B.J. Ha, "Capacitive sensing type surface micromachined silicon accelerometer with a stiffness tuning capability," *1998 Micro Electro Mechanical Systems, MEMS '98*, pp. 637–642, 1998.

[14] Y. Wang and M. Esashi, "The structures for electrostatic servo capacitive vacuum sensors," *Sensors and Actuators A: Physical*, vol. 66, pp. 213–217, 1998.

[15] B.P. Gogoi and C.H. Mastrangelo, "A low-voltage force-balanced pressure sensor with hermetically sealed servomechanism," *1999 Micro Electro Mechanical Systems, MEMS '99*, pp. 493–498, 1999.

[16] M. Elwenspoek and R. Wiegerink, *Mechanical Microsensors*, Springer-Verlag, New York, 2001.

[17] H.R. Zulliger, "Precise measurement of small forces," *Sensors and Actuators A: Physical*, vol. 4, pp. 483–495, 1983.

[18] N. Hogan, "Impedance control: an approach to manipulation," *Journal of Dynamics Systems, Measurement and Control*, vol. 107, pp. 1–24, 1985.